

Journal of Biomedical Optics

BiomedicalOptics.SPIEDigitalLibrary.org

Measurement of tissue-radiation dosage using a thermal steady-state elastic shear wave

Sheng-Yi Chang
Tung-Sheng Hsieh
Wei-Ru Chen
Jin-Chung Chen
Chien Chou

SPIE.

Sheng-Yi Chang, Tung-Sheng Hsieh, Wei-Ru Chen, Jin-Chung Chen, Chien Chou, "Measurement of tissue-radiation dosage using a thermal steady-state elastic shear wave," *J. Biomed. Opt.* **22**(8), 085001 (2017), doi: 10.1117/1.JBO.22.8.085001.

Measurement of tissue-radiation dosage using a thermal steady-state elastic shear wave

Sheng-Yi Chang,^{a,b,†} Tung-Sheng Hsieh,^{c,†} Wei-Ru Chen,^a Jin-Chung Chen,^d and Chien Chou^{a,e,f,*}

^aChang Gung University, Ph.D. Program in Biomedical, Engineering College of Engineering, Taoyuan, Taiwan

^bMing Chi University of Technology, The General Education Center, Taipei, Taiwan

^cTaipei Veterans General Hospital, Department of Oncology, Taipei, Taiwan

^dChang Gung University, Institute of Biomedical Science, Taoyuan, Taiwan

^eChang Gung University, Graduate Institute of Electro-optical Engineering, Taoyuan, Taiwan

^fChang Gung University, Center for Biomedical Engineering, Taoyuan, Taiwan

Abstract. A biodosimeter based on thermal-induced elastic shear wave (TIESW) in silicone acellular porcine dermis (SAPD) at thermal steady state has been proposed and demonstrated. A square slab SAPD treated with ionizing radiation was tested. The SAPD becomes a continuous homogeneous and isotropic viscoelastic medium due to the generation of randomly coiled collagen fibers formed from their bundle-like structure in the dermis. A harmonic TIESW then propagates on the surface of the SAPD as measured by a nanometer-scaled strain-stress response under thermal equilibrium conditions at room temperature. TIESW oscillation frequency was noninvasively measured in real time by monitoring the transverse displacement of the TIESW on the SAPD surface. Because the elastic shear modulus is highly sensitive to absorbed doses of ionizing radiation, this proposed biodosimeter can become a highly sensitive and noninvasive method for quantitatively determining tissue-absorbed dosage in terms of TIESW's oscillation frequency. Detection sensitivity at 1 cGy and dynamic ranges covering 1 to 40 cGy and 80 to 500 cGy were demonstrated. © 2017 Society of Photo-Optical Instrumentation Engineers (SPIE) [DOI: [10.1117/1.JBO.22.8.085001](https://doi.org/10.1117/1.JBO.22.8.085001)]

Keywords: viscoelastic shear wave; elastic shear modulus; polarized heterodyne interferometer; biodosimeter.

Paper 170030RRR received Jan. 15, 2017; accepted for publication Jul. 10, 2017; published online Aug. 4, 2017.

1 Introduction

A chromosome dosimeter is based on scoring dicentric and ring chromosomes in human blood lymphocytes. It is the most widely distributed and reliable biological technique in radiological protection and is used to estimate individual whole-body doses of about 100 mGy of low-linear energy transfer radiation.¹ However, this approach is limited in its detection accuracy during observation. In conventional high-speed optical three-dimensional (3-D) dosimetry, it records two-dimensional (2-D) projections of optical absorption data, and a 3-D absorbed dose distribution is derived.² An optical 3-D dosimeter follows the principles of conventional x-ray computed tomography in which a polymer gel phantom is introduced for measurement of absorbed doses. A large optical penetration depth in the polymer gel phantom is applicable. Experimentally, collagen fibers in a dermis are highly sensitive to ionizing radiation. Even at low absorbed doses, this type of radiation causes randomly coiled collagen fibers to be formed from their normal bundle-like structure.³⁻⁵ This causes the dermis to become a continuous homogeneous and isotropic viscoelastic medium. As a result, the tissue-absorbed dose can be determined by the change of dermal birefringence properties.^{6,7} Similarly, a biodosimeter for measuring tissue-absorbed doses in terms of dermal viscoelastic properties is also anticipated. To measure the dynamic response of the complex shear modulus, a method using an atomic force microscope coupled with force modulation produced

by a sinusoidal driving piezoelectric transducer has been proposed. It will be capable of properly characterizing the viscoelastic properties of a Langmuir-Blodgett film.⁸ In addition, a modified torsion pendulum in which the relative change of sample length at an order of 10^{-7} has been established, and the dynamic mechanical properties of polyvinyl acetate on complex shear modulus within the glass transition temperature was studied.⁹ Recently, optical coherence elastography (OCE) for Young's modulus generated by static or dynamic specimen loading during the course of the measurement has been proposed.¹⁰ In this study, a biodosimeter that would measure the tissue-absorbed dose in terms of porcine dermis elastic properties under thermodynamic equilibrium conditions at room temperature has been proposed. Because porcine dermis is morphologically and physiologically similar to human dermis, a silicone acellular porcine dermis (SAPD)¹¹ was chosen, and a noninvasive biodosimeter based on the measurement of nanoscale elastic properties of SAPD has been established. At present, methods for estimating the damage of skin-ionizing radiation in radiation therapy are focused on tissue slices or cell cultures.¹² A noninvasive and quantitative evaluation method on tissue-radiation damage was required and has been developed. This type of method is critical to ensure that cancer patients receive optimized treatment during radiation therapy. To expose an SAPD to ionizing radiation, it results in a continuous, isotropic and homogeneous SAPD. The viscoelastic characterization of SAPD undergoes a nanoscale strain-stress response under thermal equilibrium condition at room temperature and

*Address all correspondence to: Chien Chou, E-mail: cchou01@gmail.com

†Authors contributed equally.

the SAPD's elastic properties are only considered.^{9,13,14} As a result, the elastic property of SAPD induced by ionizing radiation is equivalent to a simple harmonic oscillator under free external driving force conditions.^{13,15} The elastic shear modulus of the SAPD can then be measured via a thermal-induced elastic shear wave (TIESW) generated in the SAPD by a two-frequency polarized heterodyne interferometer (TFPHI). The absorbed dose of ionizing radiation can be noninvasively and quantitatively evaluated in terms of the elastic shear modulus. This is in contrast to the complex shear modulus in viscoelastic media generated via complex shear wave propagation under an external driving force in which both elastic and viscous properties of the complex shear waves are considered concurrently.¹⁶ In this study, TFPHI was used to investigate the elastic shear modulus of an SAPD in terms of the oscillation frequency of a TIESW at room temperature. The transverse displacement of the TIESW on the surface of a square SAPD was measured in real time. Experimentally, a linear relationship between the absorbed dose and the oscillation frequency of TIESW was found. A detection sensitivity at 1 cGy over a wide dynamic range covering 1 to 40 cGy and 80 to 500 cGy of the absorbed dose was demonstrated.

2 Thermal-Induced Elastic Shear Waves in Viscoelastic Media

Theoretically, a TIESW is generated in an isotropic and homogeneous viscoelastic medium at room temperature under steady-state thermal equilibrium conditions.^{16,17} The wave equation for a TIESW and its speed of propagation are expressed by¹⁶

$$\frac{\partial^2 \mu_s}{\partial t^2} - v_s^2 \frac{\partial^2 \mu_s}{\partial x^2} = 0, \quad (1)$$

$$v_s = \sqrt{\frac{M}{\rho}}, \quad (2)$$

in which v_s the velocity of a TIESW in the viscoelastic medium, M is the energy stored component in a complex shear wave or elastic shear modulus, ρ is the mass density of the medium, and μ_s is the transverse displacement of the TIESW propagating along the x direction [Fig. 1(a)]. The displacement of μ_s in the y direction is expressed by $\mu_y(x, t) = c \cos(\omega t - kx)$, where k is the wave number of the TIESW and c is a constant. Accordingly, the TIESW corresponds to a simple harmonic oscillator without an external driving force.

When a square slab of an isotropic and homogeneous viscoelastic medium [Fig. 1(b)] is considered, a standing TIESW

is produced on the surface of the specimen by two counter-propagating TIESWs along the x axis. Hence, the transverse displacement of the TIESW in the y direction is expressed as

$$\begin{aligned} \mu_y(x, t) &= c \cos(k_x x - \omega_x t) + c \cos(k_x x + \omega_x t) \\ &= 2c \cos(k_x x) \cos(\omega_x t). \end{aligned} \quad (3)$$

Meanwhile, the second standing TIESW simultaneously propagating along the z axis also yields the transverse displacement in the y direction, which is expressed by

$$\begin{aligned} \mu_y(z, t) &= c \cos(k_z z - \omega_z t) + c \cos(k_z z + \omega_z t) \\ &= 2c \cos(k_z z) \cos(\omega_z t), \end{aligned} \quad (4)$$

where (k_x, ω_x) and (k_z, ω_z) were the wave number and angular frequency of the TIESWs along the x and z directions, respectively. Therefore, the total transverse displacement in the y direction by two orthogonal standing TIESWs under an inphase condition becomes

$$\begin{aligned} \mu_y &= \mu_y(x, t) + \mu_y(z, t) \\ &= 2c \left[\cos\left(\frac{\pi}{L} z\right) + \cos\left(\frac{\pi}{L} x\right) \right] \cos(\omega_0 t), \end{aligned} \quad (5)$$

in which the oscillation frequency is $\omega_x = \omega_z = \omega_0$. Both standing TIESWs are assumed to be at the lowest mode number in which the width of the square slab is equal to L . Thus, the total displacement in the y direction at a location $(x_0 = z_0)$ at the center of surface becomes

$$\mu_y = 4c \cos\left(\frac{\pi}{L} x_0\right) \cos(\omega_0 t), \quad (6)$$

$$\omega_0 = k v_s = \left(\frac{\pi}{L}\right) \sqrt{\frac{M}{\rho}}. \quad (7)$$

As a result, the oscillation frequency of a standing TIESW on the surface is linearly dependent on $M^{1/2}$ of the elastic shear modulus and inversely proportional to $\rho^{1/2}$ of the mass density of the specimen.

3 Two-Frequency Polarized Heterodyne Interferometer

Figure 2 shows the setup of a TFPHI in which a two-frequency stabilized He-Ne laser was used. The output was a pair of highly spatial and temporally correlated linearly polarized P and S light

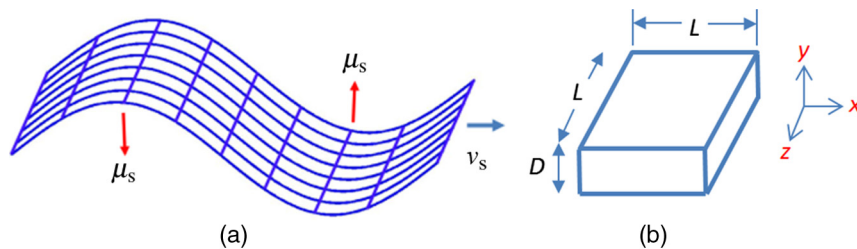


Fig. 1 (a) A TIESW on the surface of a squared slab of isotropic and homogeneous viscoelastic medium in (b).

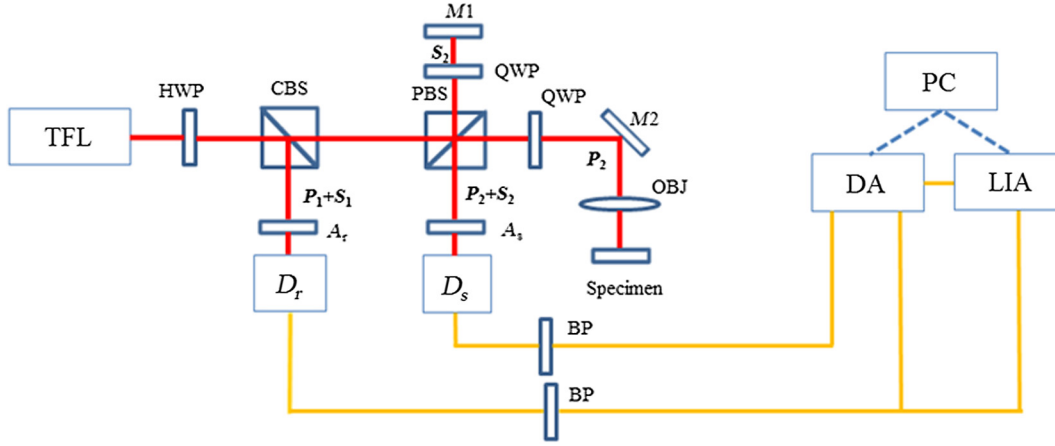


Fig. 2 Optical setup of TFPPI. TFL, two-frequency laser; HWP, half wave plate; QWP, quarter wave plate; A_r , A_s , analyzers; D_r , D_s , detectors; BP, band pass filter; OBJ, objective lens; DA, differential amplifier; LIA, lock-in amplifier.

waves at ω_p and ω_s in temporal frequency, respectively. A slight difference in temporal frequencies between ω_p and ω_s was introduced in the laser beam.

Initially, the P and S light waves were oriented along the x and y axes of the laboratory coordinates, respectively, via the use of a half-wave plate. Then, the laser beam was divided into two beams. One beam was the reference beam, and the other was the signal beam. The reference beam (P_1 and S_1) passed through an analyzer (A_r) with an azimuth angle set at φ_r , and a heterodyne signal I_r generated by photodetector D_r .

$$I_r = I_{P_1+S_1}(\Delta\omega t) = DC_1 + \sin(2\varphi_r)\sqrt{I_{P_1}I_{S_1}}\cos(\Delta\omega t + \Delta\phi_A), \quad (8)$$

in which DC_1 is the noninterference term and $\Delta\omega = |\omega_p - \omega_s|$ was the beat frequency of the signal. The signal beam was simultaneously decomposed into P_2 and S_2 polarizations laser beams in a Michelson interferometer. The P_2 wave was called the tested beam, and the S_2 wave was called the second reference beam. Each beam passed a quarter wave plate with an azimuth angle adjusted 45 deg relative to the x axis. The test and second reference beams were then recombined using a polarized beam splitter. Meanwhile, an analyzer A_s of its azimuth angle at 45 deg was positioned in the optical path before photodetector D_s . The heterodyne signal I_s from the Michelson interferometer was generated and expressed as

$$I_s = I_{P_2+S_2}(\Delta\omega t) = DC_2 + \sqrt{I_{P_2}I_{S_2}}\cos(\Delta\omega t + \Delta\phi_B), \quad (9)$$

in which DC_2 is the noninterference term. In Eqs. (8) and (9), (I_{P_1}, I_{S_1}) were the intensities of the P_1 and S_1 waves in the reference beam, respectively, and (I_{P_2}, I_{S_2}) were the intensities of the P_2 and S_2 waves in the signal beam, respectively. $\Delta\phi_A = \phi_{P_1} - \phi_{S_1}$ was the phase difference between the P_1 and S_1 waves; $\Delta\phi_B = \phi_{P_2} - \phi_{S_2}$ was the phase difference between the P_2 and S_2 waves. The azimuth angle φ_r of the analyzer in the reference beam was adjusted until the condition of equal intensity of two heterodyne signals in Eqs. (8) and (9) was satisfied $\sin(2\varphi_r)\sqrt{I_{P_1}I_{S_1}} = \sqrt{I_{P_2}I_{S_2}} = \kappa$. In addition, the DC terms in Eqs. (8) and (9) were filtered out with a band pass filter.

Two heterodyne signals were subtracted from each other using a differential amplifier (DA) and the output intensity from DA was calculated¹⁸⁻²⁰ as

$$I_{\text{out}}(\Delta\omega t) = \gamma[I_{P_1+S_1}(\Delta\omega t) - I_{P_2+S_2}(\Delta\omega t)] = \left|4\gamma\kappa \sin\left(\frac{\Delta\phi}{2}\right)\right| \sin(\Delta\omega t), \quad (10)$$

in which γ was the gain of DA and $\Delta\phi = (\Delta\phi_A - \Delta\phi_B)$ was the phase difference between the two heterodyne signals. It can clearly be seen that $I_{\text{out}}(\Delta\omega t)$ belongs to an amplitude-modulated (AM) signal whose amplitude was proportional to $|\sin(\frac{\Delta\phi}{2})|$. Because of common-path propagation of P_1 and S_1 waves, $\Delta\phi$ equaled the phase difference between P_2 and S_2 in the signal channel of the Michelson interferometer. Hence, a small transverse displacement of the test surface relative to the reference point on a plane mirror (Fig. 2) was measured in real time by monitoring the amplitude profile of the received AM signal from DA.

$$\Delta\phi = 2 \sin^{-1}\left(\frac{|I_{\text{out}}|}{4\gamma\kappa}\right). \quad (11)$$

Thus, the transverse displacement of a TIESW on the surface of a specimen was expressed as

$$\Delta h = \frac{\Delta\phi}{4\pi}\lambda = \frac{\lambda}{2\pi} \sin^{-1}\left(\frac{|I_{\text{out}}(\Delta\omega t)|}{4\gamma\kappa}\right), \quad (12)$$

in which λ is the wavelength of the laser beam.

4 Sample Preparation

In the experiment, a square slab SAPD with a 25-mm width and 0.5-mm thickness was prepared (shown in Fig. 3). In this study, SAPD was provided by the Department of Plastic and Reconstructive Surgery at Tri-Service General Hospital, Taipei, Taiwan. The protocol for preparing the SAPD was described by Wang et al.¹¹ using several steps: (1) a whole piece of porcine skin was harvested and preserved in a -70°C deep freezer; (2) a 10/1000-inch thick porcine skin was harvested to remove the epidermis, and then a 12/1000-inch porcine dermis was harvested

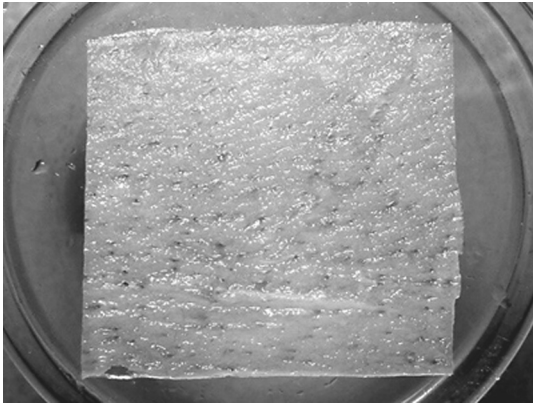


Fig. 3 Picture of squared SAPD with a 25-mm width and 0.5-mm thickness.

again; (3) the porcine dermis was treated with 1% trypsin for 1 h at ambient temperature (25°C) to remove cellular material other than porcine dermal collagen to manufacture acellular porcine dermis (APD); and (4) after the APD was dried, a piece of a 6–8/1000 inch silicone sheet (MDX-4210 A/B Dow Corning) was cross-linked by heat to bind to the surface of the APD to become the test SAPD. Conventionally, the SAPD was packed in a sealed plastic bag with 75% ethyl alcohol mixed with glycerol (v/v 9:1) and preserved in a 4°C refrigerator for future use.

5 Experimental Results

5.1 Stability of Differential-Phase Measurements of a Two-Frequency Polarized Heterodyne Interferometer

Two fixed-plane mirrors were positioned in the P_2 and S_2 waves in the TFPPI in which a two-frequency linearly polarized He–Ne 5517 laser head (Agilent Technologies) was used. The wavelength and beat frequency were 632.8 nm and 1.8 MHz, respectively. The output signal from the DA was sent into a lock-in amplifier for a system differential-phase stability test. A difference phase at 0.3 deg was attained within 10 min of the measurement (see Fig. 4). According to Eq. (12), depth resolution of the transverse displacement at 0.3 nm and the dynamic range at 150 nm were calculated.

5.2 Elastic Shear Modulus and the Oscillation Frequency of Thermal-Induced Elastic Shear Waves

In this experiment, a disk of homogeneous and isotropic gelatin with a 2-cm diameter and 2.5-cm thickness was used. Figure 5 shows the measured harmonic oscillation of the transverse displacement of the TIESW located at the center of a gelatin surface using TFPPI. According to the properties of the TIESW, only the elastic shear modulus M is considered in a continuous, isotropic, and homogeneous SAPD which has been exposed to ionizing radiation at room temperature. Experimentally, this is true for two reasons: (1) the nanometer size of collagen fibers in dermis²¹ and (2) spatial average of the spot size of the focused laser beam on the SAPD using a microscopic objective of 0.65 numerical aperture (NA) in this setup for transverse displacement measurement. Because M strongly correlates with the mechanical properties of porcine dermis, the elastic shear modulus of SAPD is changed in the presence of ionizing radiation due

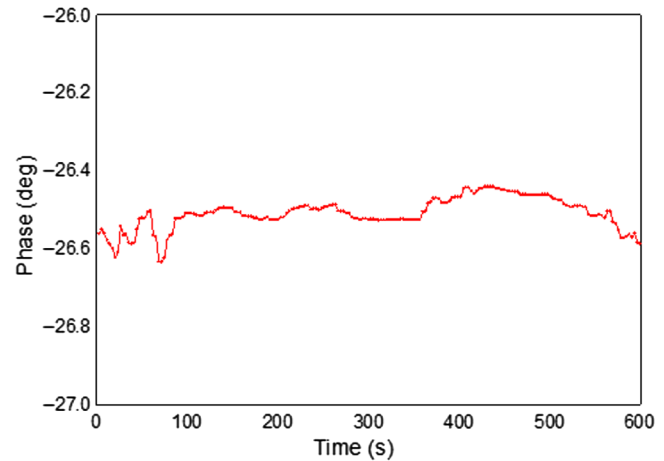


Fig. 4 Differential-phase stability of TFPPI.

to an interaction of collagen fibers in porcine dermis with high-energy photons. Even at very low absorbed doses, the photons induce randomly coiled collagen fibers in the dermis. This is in contrast to the damage-producing mechanism that affects the chemical bond in collagen fibers at high absorbed doses.^{12,22} Nevertheless, both arrangements result in an equivalent, continuous, homogeneous, and isotropic porcine dermis. Hence, the wave TIESW profile and its transverse displacement oscillation frequency on the sample surface become highly sensitive to the absorbed dose. Quantitatively, the chosen SAPD test sample was a living porcine dermis, which was suitable for noninvasive absorbed dose measurements in terms of measured TIESW harmonic oscillation frequency according to Eq. (7). In addition, we sought to monitor the changes in the TIESW wave profile from an irregular one at zero-absorbed dose under anisotropic and inhomogeneous conditions, which was then converted to a harmonic oscillation after radiation exposure. This can be a highly sensitive method for determining the absorbed dose at low absorbed doses (1 cGy). Experimentally, the SAPD of living porcine dermis at low absorbed doses undergoes nonpermanent damage, and the collagen fibers are able to return to their normal stage automatically as determined by observing the changes in the TIESW profile over time. After receiving a high absorbed dose, the porcine dermis is permanently damaged. The collagen fibers are not able to return to the normal stage, and the

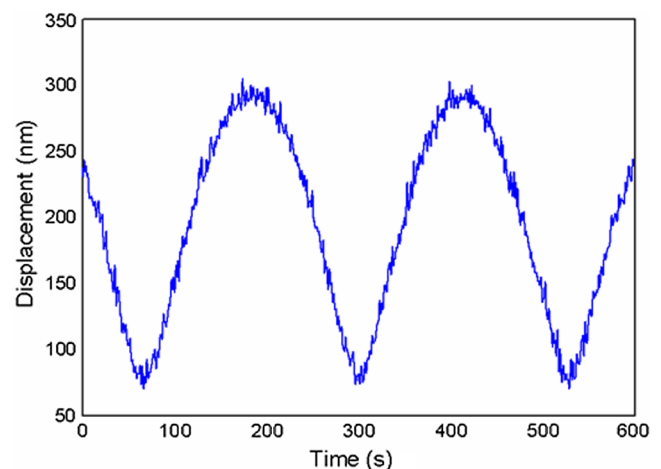


Fig. 5 Transverse displacement of TIESW on the surface of a disk of gelatin with a 2-cm diameter and 2.5-cm thickness.

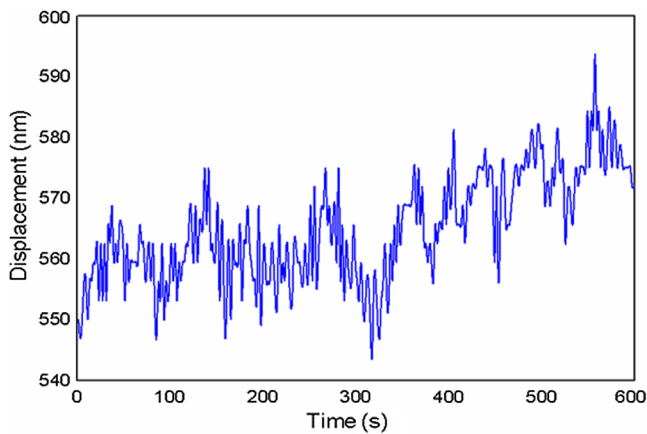


Fig. 6 Transverse displacement of a TIESW in the SAPD at room temperature before exposure to ionizing radiation.

harmonic wave profile of the measured TIESW is constant. Nevertheless, the temperature effect was ignored in this study since there is no heat absorption during ionizing radiation.

In Fig. 2, a microscopic objective (40 \times , NA = 0.65) was used to focus the P_2 wave onto the surface of the SAPD for transverse displacement measurements in real time. At first, a normal and nondenatured square SAPD (without being exposed in ionizing radiation) was tested at room temperature (26 $^{\circ}$ C). As expected, an irregular TIESW wave profile was observed as shown in Fig. 6. This is due to the inhomogeneous and anisotropic properties in the SAPD. Next, the same SAPD sample was exposed to ionizing radiation at an absorbed dose of 1 cGy of 2% uncertainty from a Cobalt-60 Tele-therapy Unit (AECL Co-60 Eldorado 78, CAN) located in the Department of Biomedical Imaging and Radiological Sciences, National Yang Ming University, Taipei, Taiwan. To precisely produce a 1-cGy absorbed dose in the SAPD, a square bolus of 5-mm thick was positioned underneath the test SAPD. To keep the SAPD in living condition, it was moistened using saline solution in a thin plastic container during the measurements. The gantry and test SAPD were established following the geometry of an inverted incidence ionizing radiation beam as shown in Fig. 7. The bolus was placed underneath the SAPD in this setup to maximize the absorbed dose by the SAPD. This arrangement assured that the absorbed dose was 1 cGy in the SAPD according to the cobalt-60 depth-dose calculation.¹²

Finally, the TIESW was measured 20 min after the SAPD had been exposed to the ionizing radiation. A harmonic TIESW oscillation is clearly shown in Fig. 8(a). This was due to a continuous, homogeneous, and isotropic SAPD produced by the 1-cGy ionizing radiation. However, the same SAPD was measured 60 min after exposure to the ionizing radiation. A conversion from a harmonic oscillation into an irregular profile was observed as shown in Fig. 8(b). These results indicate that the collagen fiber in the SAPD was able to recover its normal stage at an absorbed dose of 1 cGy. This implies that there was no permanent damage in the SAPD's collagen fibers at low absorbed doses.

Furthermore, we measured TIESW oscillation frequencies in a set of SAPD specimens with 25-mm width and 0.5-mm thickness, which were prepared under different absorbed doses using a 6MV accelerator (Varian 1800C; Varian Medical Systems) in the Department of Oncology of the Taipei Veteran General

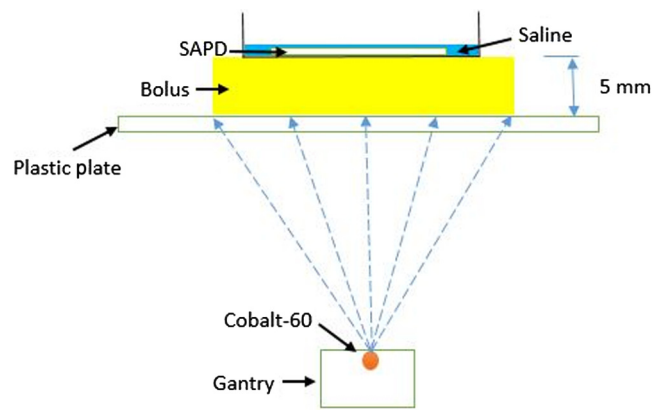


Fig. 7 Geometry of inverted incidence of the ionized radiation beam.

Hospital Taipei, Taiwan. The linear relationship between the given absorbed doses at 1, 5, 10, 20, and 40 cGy at 1.5% uncertainty and their TIESW oscillation frequencies is shown in Fig. 9. A correlation of $R^2 = 0.916$ was achieved. The detection sensitivity in this measurement was 1 cGy. At the low absorbed dose, porcine dermis becomes a homogeneous, isotropic, and continuous medium due to randomly coiled collagen fiber conversion in the dermis. The covalent bonds in the collagen fiber are not seriously damaged because of the small cross section of the dermis and the high-energy photon interaction during ionizing radiation. Concurrently, randomly coiled collagen fibers result in decreased mass density in the dermis. This is why the oscillation frequency increased in the low absorbed dose range in Fig. 9. In addition, the second set of SAPDs with the same size and thickness was tested in a high absorbed dose range using the 6MV accelerator. Figure 10 shows the linear relationship between the measured TIESW oscillation frequency and the absorbed doses at 80, 100, 150, 200, 250, 300, 400, and 500 cGy in which the absorbed dosage uncertainty was 1.5%. The correlation was $R^2 = 0.894$. This result agrees well with previously published results concerning gelatin, which was rigidly degraded in the presence of ionizing gamma radiation at 20 MGy.²³ The reason for the linear negative slope response in the highly absorbed dose range compared with the positive slope linear response obtained in low absorbed dose range appears to be due to severe damage of collagen fibers in the dermis in which the chemical bonds were broken during radiation exposure. This lowers the elastic shear modulus of the dermis while the SAPD mass density remains the same as shown in the low absorbed homogeneous and isotropic dose. Quantitatively, the results of the SAPD's oscillation frequency in the 1 to 40 cGy dose range are influenced by mass density, whereas the elastic shear modulus is influenced in the 80 to 500 cGy region. In addition, the SAPD would be unable to recover back to its normal condition if the damage was produced at a highly absorbed dose and is then permanent damaged. Figure 11 shows the evidence of the measured TIESW profile 24 h after the specimen had been exposed to radiation at a high absorbed dose. From these results, we predicted that all SAPD specimens in the 1 to 40 cGy absorbed dose range in Fig. 9 would be capable of recovering to their normal stages since no severe damage to their elastic shear modulus occurred. All SAPD specimens lost the capability to recover back to their normal stages in the 80 to 500 cGy absorbed dose range due to severe and permanent damage of the elastic shear modulus generated in the collagen fibers.

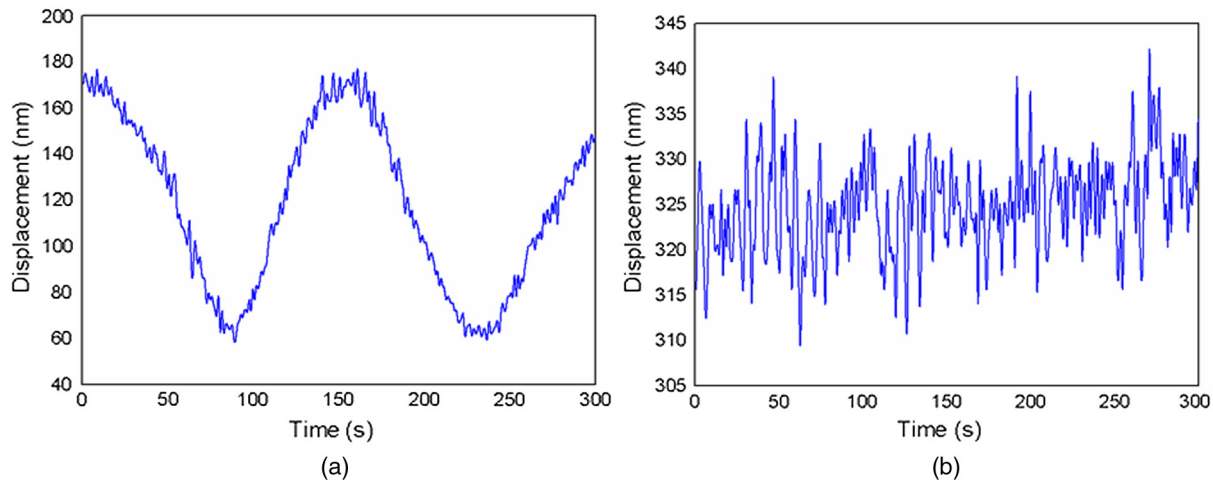


Fig. 8 TIESW on the surface of a squared SAPD at 1 cGy: time to measure at (a) 20 min and (b) 60 min after being exposed to ionized radiation.

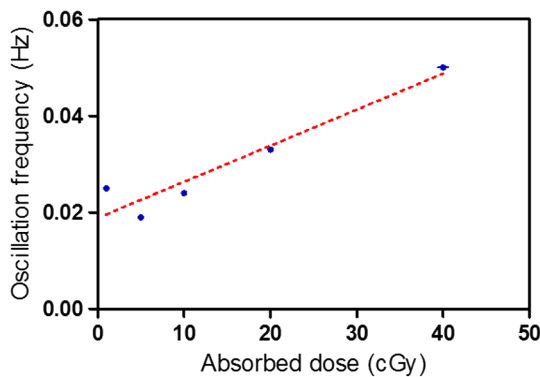


Fig. 9 Oscillation frequency of TIESW in SAPD at low absorbed dose in a range of 1 to 40 cGy.

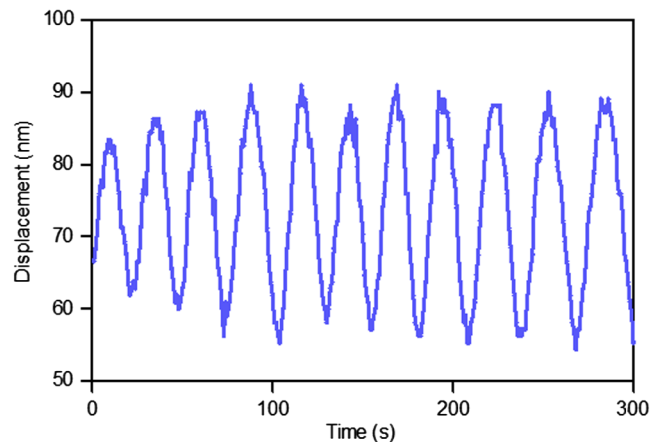


Fig. 11 TIESW profile of a SAPD 24 h after being exposed to radiation under highly absorbed dose with permanent damage.

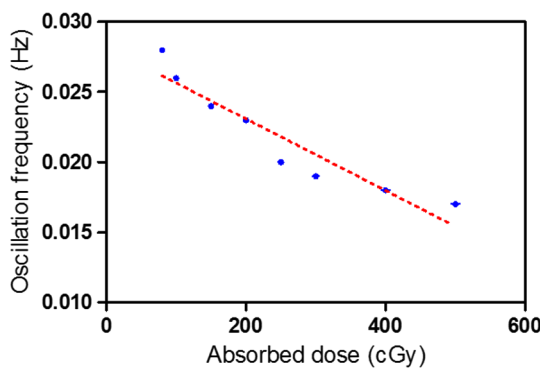


Fig. 10 Oscillation frequency of a TIESW in SAPD at highly absorbed doses in the range of 80 to 500 cGy.

We also established one-dimensional (1-D) absorbed dose distribution measurements as shown in Fig. 12. Five different absorbed doses at different locations in the SAPD were established using a 6MV linear accelerator. To avoid the source penumbra effect, the specimen was separated into five areas and exposed to the different doses listed in Fig. 12(a).^{12,24}

In the measurement, the SAPD was separately exposed over five different regions following sequential exposures at 20, 40, and 60 cGy. Figure 12(b) presents the corresponding 1-D dose distribution in the SAPD in terms of the TIESW oscillation frequency. The consistency between the designed absorbed dose in Fig. 12(a) and the measured absorbed dose in Fig. 12(b) is clearly shown. This result indicates the possibility that a 1-D or even 2-D dose distribution can be obtained by the TIESW method, which is especially useful in treatment planning for cancer patients undergoing radiotherapy.²⁵

6 Discussion and Conclusions

Porcine dermis is very sensitive to ionizing radiation, which makes it possible not only to induce continuation, homogeneity, and isotropy in the dermis but also to change its elastic shear modulus due to interactions with high-energy photons. When detection with a microscopic objective ($NA = 0.65$) at micrometer lateral resolution for transverse displacement TIESW measurements in this experiment was done, the assumption of a continuous, isotropic, and homogeneous viscoelastic medium of SAPD becomes applicable due to the spatial average in the spot size area of the focused laser beam. A harmonic TIESW

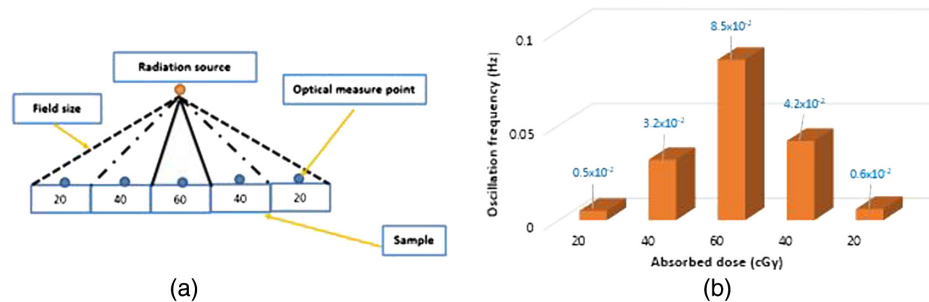


Fig. 12 (a) Setup of 1-D dose distribution in an SAPD at a given exposure of ionizing radiation and (b) the measured 1-D absorbed dose distribution versus TIESW oscillation frequency.

can then be generated on the surface of the SAPD at room temperature under thermal equilibrium conditions. Because no heat absorption is produced during ionizing radiation, the TIESW oscillation frequency at room temperature is only dependent on the absorbed dose. Our experiment showed that the oscillation frequency of a TIESW became linearly dependent on the absorbed dose over a widely absorbed dose range. Qualitatively, the detection sensitivity at 1 cGy was demonstrated by directly monitoring the TIESW harmonic profile conversion from its irregular shape under zero-absorbed dose at normal stage. Quantitatively, the linear dependence of the absorbed dose and oscillation frequency of the TIESW was clearly observed and measured at both the 1 to 40 cGy and 80 to 500 cGy dose ranges. The spatial resolution of the TFPHI in the micrometer range does not influence the elastic shear modulus detection due to the transverse displacement measurement of TIESW at nanometer detection sensitivity. Meanwhile, the capability to convert the SAPD from inhomogeneous and anisotropic in its normal stage to homogeneous and isotropic at low absorbed doses provides a very sensitive method to judge radiation exposure during the very early stages. The detection sensitivity at 1 cGy in this method is 10-fold higher for detection sensitivity than the conventional biodosimeter at 100 mGy based on chromosome aberration analysis and optical 3-D dosimeter.^{1,2,26} Moreover, by directly monitoring the change in the TIESW profile in real time, it is capable of measuring the transit stage of the dermis during ionizing radiation. In addition, from the positive or negative slope of linear dependence between the absorbed dose and the oscillation frequency of the TIESW in these experiments, it was possible to predict the recovery abilities of a living porcine dermis treated with ionizing radiation. In this study, measuring tissue-absorbed dose in terms of elastic shear modulus using TFPHI was motivated by optical interferometry features with (1) noninvasive and (2) high detection sensitivity. The findings that dermal collagen fibers are highly sensitive to ionizing radiation that induce morphological changes at low absorbed dose and changes in elastic shear modulus of the collagen fibers at high absorbed dose are also integral steps in this method. They can be used for retrospective radiation dose assessment in radiation biodosimetry due to the correlation between the elastic shear modulus and the accumulated absorbed dose. Moreover, this setup using the SAPD can also improve the efficiency of clinical treatment in radiotherapy for the evaluation of skin radiation damage *ex vivo*. It appears to be able to prevent destructive and permanent skin damage during treatment. Furthermore, to compare the proposed method with the conventional high-speed optical 3-D dosimetry² using polymer gels for absorbed dose measurement, 2-D projections of optical absorption data in a

polymer gel phantom were used. In addition, the measurement speed in this setup relies on the speed of propagation of TIESW on the interface. Experimentally, it took several minutes before we were able to determine the oscillation frequency of TIESW in each measurement. This is not comparable to the conventional high-speed optical 3-D dosimetry used in radiotherapy. In this study, we demonstrated single-point and 1-D measurements rather than 2-D or 3-D distribution of the absorbed dose measurement. Nevertheless, this technique can be extended into 2-D dose distribution if an x - y scanner is used in the TFPHI for TIESW measurements. Meanwhile, 3-D dose distribution in a specimen might be anticipated if a low coherence laser diode is used in TFPHI due to the localization ability in a low coherence volume in the specimen and the TIESW is assumed to exist on the interfaces in the specimen. Hence, a TIESW-based method can be considered as an optical coherence biodosimeter, which is similar to the conventional OCE setup for soft tissue.^{27,28} The potential applications in the areas of soft material and biological sciences for general radiation exposure measurements are also promising.

Disclosures

No conflicts of interest, financial or otherwise, are declared by the authors.

Acknowledgments

This research was partially supported by the Ministry of Science and Technology (MOST) of Taiwan. The authors express their gratitude to the Department of Oncology of Taipei Veteran General Hospital in Taipei, Taiwan, for providing the 6MV Linear Accelerator (Varian 1800C) and also the Department of Biomedical Imaging and Radiological Sciences, National Yang Ming University, Taipei, Taiwan, for Cobalt-60 Teletherapy Unit (AECL Co-60 Eldorado 78, CAN) as the ionizing radiation sources. Meanwhile, we gratefully recognize support from Dr. S.-J. Wang from Plastic and Reconstructive Surgery at Tri-Service General Hospital in Taipei, Taiwan, for providing the SAPD in this study.

References

1. M. Bauchinger, "Quantification of low-level radiation exposure by conventional chromosome aberration analysis," *Mutat. Res.* **339**, 177–189 (1995).
2. C. Baldock et al., "Polymer gel dosimetry," *Phys. Med. Biol.* **55**(5), R1 (2010).
3. D. C. Lloyd et al., *Cytogenetic Analysis for Radiation Dose Assessment a Manual*, pp. 14–24, International Atomic Energy Agency, Vienna (2001).

4. H. S. Ranu, T. E. Burlin, and W. C. Hutton, "The effects of x-irradiation on the mechanical properties of skin," *Phys. Med. Biol.* **20**, 96–105 (1975).
5. R. A. Grant and R. W. Cox, "The effect of gamma irradiation on the structure and reactivity of native and cross-linked collagen fibers," *J. Anat.* **115**, 29–43 (1973).
6. S. Thomsen, J. A. Pearce, and W. F. Cheong, "Changes in birefringence as makers of thermal damage in tissues," *IEEE Trans. Biomed. Eng.* **36**, 1174–1179 (1989).
7. D. J. Maitland and J. T. Walsh Jr., "Quantitative measurement of linear birefringence during heating of native collagen," *Laser Surg. Med.* **20**, 310–318 (1997).
8. M. Radmacher, R. W. Tillmann, and H. E. Gaub, "Imaging viscoelasticity by force modulation with the atomic force microscope," *Biophys. J.* **64**(3), 735–742 (1993).
9. A. J. Kovacs, R. A. Stratton, and J. D. Ferry, "Dynamic mechanical properties of polyvinyl acetate in shear in the glass transition temperature range," *J. Phys. Chem.* **67**, 152–161 (1963).
10. K. M. Kennedy et al., "Analysis of mechanical contrast in optical coherence elastography," *J. Biomed. Opt.* **18**(12), 121508 (2013).
11. H.-J. Wang et al., "The application of new biosynthetic artificial skin for long-term temporary wound coverage," *Burns* **31**, 991–997 (2005).
12. F. Khan, *The Physics Radiation Therapy*, 5th ed., p. 554, Lippincott Williams & Wilkins, Philadelphia (2016).
13. H. D. Young, R. A. Freedman, and A. L. Ford, *Sears and Remansky's University Physics with Modern Physics*, 13th ed., pp. 437–460, Springer-Verlag, New York (2012).
14. R. Marsland, III, H. R. Brown, and G. Valente, "Time and irreversibility in axiomatic thermodynamics," *Am. J. Phys.* **83**(7), 628–634 (2015).
15. G. E. Uhlenbeck and G. W. Ford, *Lectures in Statistical Mechanics*, p. 5, American Mathematical Society, Providence, Rhode Island (1963).
16. R. D. Borchardt, *Viscoelastic Waves in Layered Media*, pp. 1–18, Cambridge University Press, New York (2009).
17. Y. C. Fung, *Biomechanics: Mechanical Properties of Living Tissues*, 2nd ed., pp. 23–65, Springer-Verlag, New York (1993).
18. C. Chou, C. W. Lyu, and L. C. Peng, "Polarized differential-phase laser scanning microscope," *Appl. Opt.* **40**, 95–99 (2001).
19. C. C. Tsai et al., "High speed interferometric ellipsometer," *Opt. Express* **16**, 7778–7788 (2008).
20. C. Chou et al., "Balanced detector interferometric ellipsometry," *J. Opt. Soc. Am. A* **23**, 2871–2879 (2006).
21. N. Adams, "Radiation-induced skin reactions 2: development of a measurement tool," *Br. J. Nurs.* **8**, 1208–1211 (1999).
22. D. A. Casciato and M. C. Territo, *Manual of Clinical Oncology*, 6th ed., pp. 36–40, Wolters Kluwer Health/Lippincott Williams & Wilkins, Philadelphia (2009).
23. A. R. Fassih and M. S. Parker, "Influence of gamma radiation on the gel rigidity index and binding capability of gelatin," *J. Pharm. Sci.* **77**, 876–879 (1988).
24. M. M. Urie et al., "Proton beam penumbra: effects of separation between patient and beam modifying devices," *Med. Phys.* **13**, 734–741 (1986).
25. D. Wolff et al., "Volumetric modulated arc therapy (VMAT) vs. serial tomotherapy, step-and-shoot IMRT and 3D-conformal RT for treatment of prostate cancer," *Radiother. Oncol.* **93**, 226–233 (2009).
26. M. Vaiente et al., "Fricke gel dosimeter with improved sensitivity for low-dose-level measurements," *J. Appl. Clin. Med. Phys.* **17**(4), 402–417 (2016).
27. H. J. Huang et al., "Analog differential-phase detection in optical coherence reflectometer," *Opt. Express* **16**, 12847–12858 (2008).
28. C. H. Li, Z. H. Huang, and R. K. Wang, "Elastic properties of soft tissue-mimicking phantoms assessed by combined use of laser ultrasonics and low coherence interferometry," *Opt. Express* **19**(11), 10153–10163 (2011).

Sheng-Yi Chang received his BS degree in applied physics and MS degree in physics from TamKang University, Taipei, Taiwan, in 1991 and 1994, respectively. Since 1996, he has been a lecturer of the General Education Center, Ming Chi University of Technology, Taipei, Taiwan.

Tung-Sheng Hsieh received his AS degree from Yuanpei University of Medical Technology, Hsinchu, Taiwan, in 1994 and his MS degree from Institute of Radiological Sciences, School of Medical Technology and Engineering, National Yang-Ming University in 2003. He was a radiotherapist in the Department of Radiology Oncology Taipei Veterans General Hospital (TVGH) from 1994 to 2003. Since 2004, he has been a medical physicist in the Department of Radiology Oncology in TVGH, Taiwan.

Wei-Ru Chen received his BS degree in electro-optical engineering from National United University, Miaoli, Taiwan, in 2010 and his MS degree from Graduate Institute of Electro-Optical Engineering, Chang Gung University, Taoyuan, Taiwan, in 2013. Since 2013, he has been a student of PhD program in biomedical engineering from Chang Gung University, Taoyuan, Taiwan.

Jin-Chung Chen received his BS degree in zoology from National Taiwan University, Taipei, Taiwan, in 1979 and his MS and PhD degrees in physiology and biophysics from the University of Illinois at Urbana-Champaign in 1983 and 1987, respectively. From 1987 to 1992, he was a postdoctor and an instructor in the Department of Pharmacology. Since 2003, he has been an associate professor in the Department of Pharmacology and became chairman and professor, and a director of biomedical sciences at the Chang-Gung University, Taoyuan, Taiwan. His research interests include neuropharmacology and neuroscience in drug addiction, Parkinson disease, learning and memory, and psychiatric disorders.

Chien Chou received his BS degree in physics from Chung Cheng Institute of Technology, Taiwan, in 1969, his MS degree in optics from Institute of Optics, University of Rochester in 1975, and PhD in biomedical optics from Optical Science Center, University of Arizona in 1978. He was a professor in the Department of Biomedical Imaging and Radiological Sciences, National Yang-Ming University, Taiwan. Since 2010, he has been a professor with the Graduate Institute of Electro-Optical Engineering, Chang Gung University, Taiwan. Currently, he is an adjunct professor in the same institute. His research interests include surface plasmon resonance biosensor and laser scanning confocal microscopy.